SCIENTIFIC Publishing Limited

Trends in Immunotherapy

https://ojs.ukscip.com/index.php/ti

Article

Modified Wumei Pills: Network Pharmacology and Bioinformatics in Colon Cancer Treatment

Shichao Liu [1*], Guancheng Liu [2], Chen Li [3] and Rui Zhang [4]

[1] College of Veterinary Medicine, Northeast Agricultural University, Harbin 150030, China

[2] International Cultural and Educational College, Northeast Agricultural University, Harbin 150030, China

[3] School of Basic Medical Sciences, Harbin Medical University, Harbin 163711, China

[4] School of Economics, Business and Management, Heilongjiang University, Harbin 150006, China

[*] Correspondence: LSC10251025@163.com

Received: 27 January 2025; **Revised:** 18 February 2025; **Accepted:** 24 February 2025; **Published:** 28 February 2025

Abstract: This study investigates the therapeutic mechanisms of modified Wumei pills in colon cancer treatment, utilizing network pharmacology and bioinformatics to uncover the active ingredients and their corresponding targets that intersect with colon cancer-related genes.We identified the active components of Wumei pills using the TCMSP database and predicted their targets with Swiss Target Prediction. Disease-related targets were identified through GeneCards and Disgenet. Network analysis, GO, KEGG, and PPI network construction were performed. Immunohistochemical assessments validated gene expression patterns, and ROC curve and Cox regression analyses evaluated the prognostic significance and patient prognosis correlation.The study revealed 112 common targets associated with colon cancer, with six key genes (ADRA2B, CXCR3, CYP19A1, NR1H2, PAPPA, PGR) prioritized. Functional enrichment analyses indicated significant associations with biological processes and pathways related to colon cancer. Immunohistochemical assessments confirmed the expression patterns of these genes within colon cancer tissues. ROC curve analysis highlighted the prognostic significance of the PGR gene, while molecular docking and molecular dynamics simulation studies demonstrated robust binding affinity of active components to their targets, particularly Diop with CXCR3.The research provides a scientific framework for the application of modified Wumei pills in colon cancer management, identifying potential key genes and pathways. The findings suggest that these pills could influence tumor growth and the immune microenvironment, offering novel insights for targeted therapy and immunotherapy in colon cancer treatment.

Keywords: Modified Wumei Pill; Colon Cancer; Network Pharmacology; Bioinformatics; Molecular Docking

1. Introduction

Colorectal cancer (CRC) represents one of the most prevalent malignant tumors globally, posing a significant threat to human health due to its high incidence and mortality rates. Despite advancements in modern medical interventions, including surgery, chemotherapy, and targeted therapy, the prognosis for patients diagnosed at advanced stages remains unfavorable. Consequently, the identification of novel therapeutic approaches is crucial for enhancing the quality of life and extending the survival of affected individuals. Traditional Chinese Medicine (TCM) has increasingly emerged as a focal point of research, owing to its distinctive treatment philosophy and demonstrated efficacy [1, 2].

Jiawei Wumei Wan (JWWMW) is a compound formulation derived from the traditional Chinese herbal formula Wumei Wan, which has demonstrated potential efficacy in the treatment of colorectal diseases. However, there is a notable deficiency in systematic research and detailed exploration regarding the specific mechanisms by which the modified Wumei pill exerts its effects in the treatment of colorectal cancer [3, 4].

Network pharmacology, as an emerging research methodology, offers a novel perspective for the treatment of complex diseases by elucidating the network relationships among drugs, targets, and diseases. When integrated with bioinformatics tools and methodologies, it facilitates a comprehensive analysis and prediction of the mechanisms of action of the active constituents of drugs, thereby uncovering their potential pathways for disease treatment [5, 6]. The objective of this study was to investigate the molecular mechanisms underlying the efficacy of the modified Wumei pill in the treatment of colorectal cancer, utilizing network pharmacology and bioinformatics approaches. This research aims to contribute additional insights and strategies for the management of colorectal cancer [4, 7].

This study aims to investigate the mechanisms by which modified Wumei pills exert their therapeutic effects in the treatment of colorectal cancer. The research methodology comprises several key steps: First, the active components of modified Wumei pills were identified using the Traditional Chinese Medicine System Pharmacological Database and Analysis Platform (TCMSP), followed by the prediction of their corresponding biological targets. Second, disease-related targets associated with colon cancer were identified through various disease-related databases, including GeneCards and Disgenet. A "drug-active ingredient-target-disease" network was subsequently constructed to elucidate common targets. The network was visualized using Cytoscape software, which facilitated the identification of key target genes based on network topology parameters. Additionally, Gene Ontology (GO) functional annotation and Kyoto Encyclopedia of Genes and Genomes (KEGG) pathway enrichment analyses demonstrated significant enrichment of these target genes across biological processes, cellular components, molecular functions, and signaling pathways pertinent to colorectal cancer [3]. Prognostic analyses of target genes, survival mapping, and assessments of immune-associated cells and their microenvironments were conducted using bioinformatics approaches. Finally, molecular docking techniques were employed to predict the binding affinities of the active ingredients with target proteins, thereby providing a scientific basis for understanding the mechanisms of action of modified Wumei pills in the treatment of colorectal cancer [4, 8].

2. Methodology

2.1. Screening of Active Ingredients of Supplemented Wumei Pills and Prediction of Corresponding Targets

To conduct a comprehensive analysis, input the following herbal names into the Herb Name field of the TCMSP database and analysis platform (https://old.tcmsp-e.com/tcmsp.php): "Wumei, asylum, dried ginger, angelica siriasis, Aconitum Aconitum, laurel twigs, Phellodendron Phellodendron, Coptis chinensis, and ginseng. The ADME parameters to the following criteria: Oral bioavailability (OB) greater than 30% and drug-likeness (DL) greater than 0.18, in order to screen for effective active ingredients. Subsequently, access the PubChem database (https://pubchem.ncbi.nlm.nih.gov/) to search for the SMILES representations corresponding to the active ingredients of Paeony. Finally, utilize the Swiss Target Prediction database (http://swisstargetprediction.ch/) to forecast the corresponding targets of the effective active ingredients found in the flavored plum pill.

2.2. Colon Cancer Disease-Related Target Screening

Using GeneCards (https://www.genecards.org/) data library, screening liver fiber Disgenet database corresponding targets, filtered "colon cancer" as keywords.

2.3. "Drug - Active Ingredient - Target - Disease" Network Construction

Utilizing the Venny Venny platform (https://bioinfogp.cnb.csic.es/tools/), a mapping of common targets associated with cherry and plum pills in relation to colon disease was conducted. The data pertaining to the shared targets were imported into Cytoscape version 3.9.0 to construct a network diagram illustrating the relationships among the "Supplemented Wumei Pill, active ingredients, targets, and colon cancer" for further analysis. The

size of the nodes in the network was differentiated based on the Degree value; nodes with higher Degree values were deemed more significant within the network.

2.4. PPI Network Construction

The data pertaining to the common target of the aforementioned supplemented Wumei pill and colon cancer were imported into the STRING database (https://cn.string-db.org/), utilizing Homo sapiens as the organism and setting the confidence level to medium (0.400) to construct the protein-protein interaction (PPI) network. Subsequently, the TSV file was downloaded and imported into Cytoscape version 3.9.0 for topological parameter analysis. The node sizes were selected based on the Degree value, with higher Degree values indicating a more prominent position of the node within the network.

2.5. GO Functional Annotation and KEGG Pathway Enrichment Analysis

The analysis of cherry and plum extracts in relation to common targets associated with colon cancer was conducted using the DAVID database (https://david.ncifcrf.gov/). The analysis focused on species with a significance threshold set at $P < 0.01$, encompassing Biological Processes (BP), Cellular Components (CC), and Molecular Functions (MF) as defined in Gene Ontology (GO) analysis, as well as pathways identified in the KEGG database. Following the removal of non-significant results, a visual representation of the data was generated using a Microscopic Application Letter (http://www.bioinformatics.com.cn/), which included a bubble chart. In this chart, the color variations of the P-values correspond to each node, while the size of the bubbles reflects the number of associated genes. Additionally, a pathway network diagram was constructed, indicating that pathways with a greater number of intersecting genes are deemed more significant, thereby increasing the likelihood of their occurrence. The top ten pathways enriched in GO categories of BP, CC, and MF were illustrated in a bar graph format, where larger bars indicate greater significance of the respective pathways.

2.6. Immunohistochemistry Based on HPA Database

The six critical target genes were input into the HPA database, and the immunohistochemical images of the six target genes in colon cancer were obtained through HPA database.

2.7. ROC Curve

The analysis was conducted using R version 4.2.1, employing the pROC package (version 1.18.0) for Receiver Operating Characteristic (ROC) analysis and the ggplot2 package (version 3.4.4) for data visualization. The pROC package automatically adjusts the outcome order of the data to ensure that the results are convex. The selected molecules were derived from gene expression data corresponding to six target points, which were obtained from the TCGA database (https://portal.gdc.cancer.gov). Specifically, the analysis focused on the TCGA-COAD (colon) project, utilizing STAR-processed RNA sequencing data and extracting it in Transcripts Per Million (TPM) format. The data filtering strategy employed was minimal, and the data processing method utilized was log2(value + 1).

2.8. KM Curve

The analysis was performed utilizing R version 4.2.1, in conjunction with several R packages: survival (version 3.3.1), curvilinear (version 0.4.9), and ggplot2 (version 3.4.4). Specifically, the survival package was employed to evaluate the proportional hazards assumption and to conduct a survival regression analysis, with the results being visualized through the integration of both the survival and ggplot2 packages. When the optimal grouping method was required, the surv_cutpoint function from the survival package was used to determine the optimal cut-off points for grouping. The Cox regression model was applied, focusing on six target genes. The prognostic outcomes examined encompassed Progression-Free Interval (PFI), Disease-Specific Survival (DSS), and Overall Survival (OS).

The expression data were sourced from the TCGA database (available at https://portal.gdc.cancer.gov). RNA sequencing data from the TCGA colon project were specifically downloaded and organized, with the data extracted in Transcripts Per Million (TPM) format. During data extraction, samples lacking clinical information were

discarded, while those relevant to colon cancer types were retained. The data filtering strategy involved the removal of normal samples and those lacking quantifiable information. The data processing method employed was log2(value + 1).

2.9. Expression Difference between Disease and Non-Disease, Heat Map of Gene Expression

The analysis was conducted using R software version 4.2.1. Data were obtained from the TCGA database (https://portal.gdc.cancer.gov), specifically focusing on the TCGA colon cancer project. The STAR process was employed to download and organize RNA sequencing data, with the aim of extracting data in Transcripts Per Million (TPM) format. During the data extraction process, samples lacking clinical information were excluded, while those corresponding to colon cancer types with quantifiable data were retained in the quantifiable information. Data filtering strategy: Remove routine + remove no clinical information. Data processing method: log2(value+1), input genes were six target genes, sample size was divided into scatter points, and results were generated by violin graph, where asterisks represented significant differences. Use ComplexHeatmap package for heat map visualization, normalization processing: row normalization, row clustering: euclidean, column clustering: non-clustering, expression data acquisition: From TCGA database (https://portal.gdc.cancer.gov) to download and organize TCGA - COAD (colon) project STAR process RNAseq data and extract the TPM data format, data filtering strategy: no, the data processing methods: log2(value+1).

2.10. Lollipop Chart of Immune Infiltration Correlation

The analysis was executed using R version 4.2.1, with the ggplot2 package (version 3.4.4) employed to conduct a correlation analysis between the primary variable in the dataset and the immune infiltration matrix data. The results were visualized using the ggplot2 package. The statistical method utilized was Spearman's correlation, while immune infiltration was assessed using the ssGSEA algorithm provided by the GSVA package (version 1.46.0). This study employed markers for 24 distinct types of immune cells, to calculate the immune infiltration corresponding to the cloud data. The specific 24 immune cell types were identified, and the data were sourced from the TCGA database (available at https://portal.gdc.cancer.go).

The RNA-seq data from the TCGA-COAD (colon) project were downloaded and organized, with the TPM format of the data and clinical data extracted. The data filtering strategy involved the removal of normal samples, and the data processing method applied was log2(value + 1).

2.11. Immunoinfiltration Correlation Heat Map

The analysis was carried out using R version 4.2.1 in conjunction with the ggplot2 package (version 3.4.4). A correlation analysis was conducted to examine the relationship between the variables within the dataset and the immune infiltration matrix data. The results were subsequently visualized via a heatmap. Spearman's correlation was employed as the statistical method. The immune infiltration was evaluated using the ssGSEA algorithm from the GSVA package (version 1.46.0) [10]. This study specifically utilized markers for 24 distinct types of immune cells, to calculate the immune infiltration corresponding to the cloud data for these 24 immune cell types.

2.12. COX Regression Results

The analysis was executed using R version 4.2.1, integrated with several R packages: survival (version 3.3.1), curvilinear (version 0.4.9), and ggplot2 (version 3.4.4). Specifically, the survival package was utilized to evaluate the proportional hazards assumption and to conduct a survival regression analysis. The results were visualized through the combined use of the survival and ggplot2 packages. When the optimal grouping method was required, the surv_cutpoint function from the survival package was employed to determine the optimal cut-off points for grouping. The statistical method applied was Cox regression, with a focus on six target genes.

The expression data were sourced from the TCGA database (available at https://portal.gdc.cancer.gov). RNA sequencing data from the TCGA colon project were specifically downloaded and organized in STAR process format, with the data extracted in Transcripts Per Million (TPM) format. During data extraction, samples lacking clinical information were excluded, while those corresponding to colon cancer types with quantifiable data were retained.

2.13. Immune Stack Bar Chart

The analysis was conducted using R version 4.2.1, along with the ggplot2 package (version 3.4.4) and the graduation package (version 0.12.3). Following the grouping of the principal variables, relevant statistical analyses were performed to determine the proportion of each group within each classification. The resulting statistics were visualized using superimposed bar charts generated by the ggplot2 package. The immune infiltration analysis was based on the core algorithm of CIBERSORT, utilizing the CIBERSORTx website (https://cibersortx.stanford.edu/) to provide markers for 22 distinct types of immune cells, which were employed to calculate immune infiltration from the uploaded data.

2.14. Single Cell Enrichment Map

Access the Human Protein Atlas (HPA) database, a comprehensive resource that consolidates protein expression data across various tissues and cell types. Within the HPA database, the expression data for proteins in distinct cell types were generated by selecting individual cell columns. Subsequently, users should input the names or identifiers of the targeted genes to query their expression across different cell types and gather the relevant data. Utilizing this data, it is possible to create enrichment maps, such as heat maps or scatter plots, to visualize the expression levels of genes in various cell types. Furthermore, statistical analyses were conducted, including the calculation of statistical differences in expression levels and correlation analyses, to assess the significance of gene expression. Ultimately, based on the results of the enrichment maps and statistical analyses, the expression patterns of the target genes in single cells were elucidated, and their biological significance was discussed.

2.15. Screening Drug Targets and Target Gene Docking

To identify the appropriate compound, access the PubChem database using either the Compound Identifier (CID) or the name of the drug ingredient. Once on the compound details page, download the Structure Data File (SDF). Subsequently, convert the SDF file into Protein Data Bank (PDB) format utilizing Open Babel software. Next, navigate to the UniProt database to locate the corresponding protein entry by searching with the name or identifier of the target gene. On the protein entry page, download the file in PDB format. Employ UCSF Chimera to eliminate water molecules and extraneous heteroatoms from the protein PDB file, thereby retaining only the protein structure. The atomic charge of the protein was estimated using the AMBER99SB force field, and the pKa values of the amino acids were calculated and assigned using the H++3 online tool. For small molecules, RDKit was utilized to generate three-dimensional structures, followed by conformation sampling. The conformations were optimized using the MMFF94 force field, and low-energy conformations were outputted. Finally, UCSF Chimera was employed to assign AM1-BCC local charges. Molecular docking experiments were conducted using AutoDock Vina software. SiteMap software was used to predict the optimal binding site and to define the docking center and box size. The conformations were ranked based on the docking score, and the best conformation was selected. The binding interactions between small molecule drug components and protein targets were analyzed. A negative binding energy indicated a significant interaction, whereas a positive value suggested a lack of meaningful binding. The calculation of binding energy is based on the scoring function of the molecular docking software, which reflects the strength of the interaction between the ligand and the receptor.

3. Results

3.1. Target Screening and Network Construction Diagram

As illustrated in **Figure 1**, a total of 126 chemical components from supplemented Wumei pills were identified in the Traditional Chinese Medicine Systems Pharmacology (TCMSP) database. The parameters for Absorption, Distribution, Metabolism, and Excretion (ADME) were established with a threshold of oral bioavailability (OB) greater than 30% and drug-likeness (DL) exceeding 0.18. The screening process yielded 8 chemical components from Wumei, 8 from Asylum, 5 from dried ginger, and 2 from Angelica. Additionally, 22 chemical components were identified from Aconite, 7 from Cassia twig, 39 from Phellodendron, 13 from Coptis, and 21 from Ginseng. Ultimately, 8 chemical components were selected as active ingredients based on an oral bioavailability (OB) threshold of greater than 36%, which included compounds such as Diop, Stigmasterol, Beta-sitosterol, Inermin, Chrysanthemaxanthin, Celabenzine, Deoxyharringtonine, and Dianthramine. These 8 effective active ingredients were subsequently en-

tered into the Swiss Target Prediction database to identify the corresponding targets associated with the active ingredients of modified Wumei pills, resulting in the identification of 305 relevant genes.

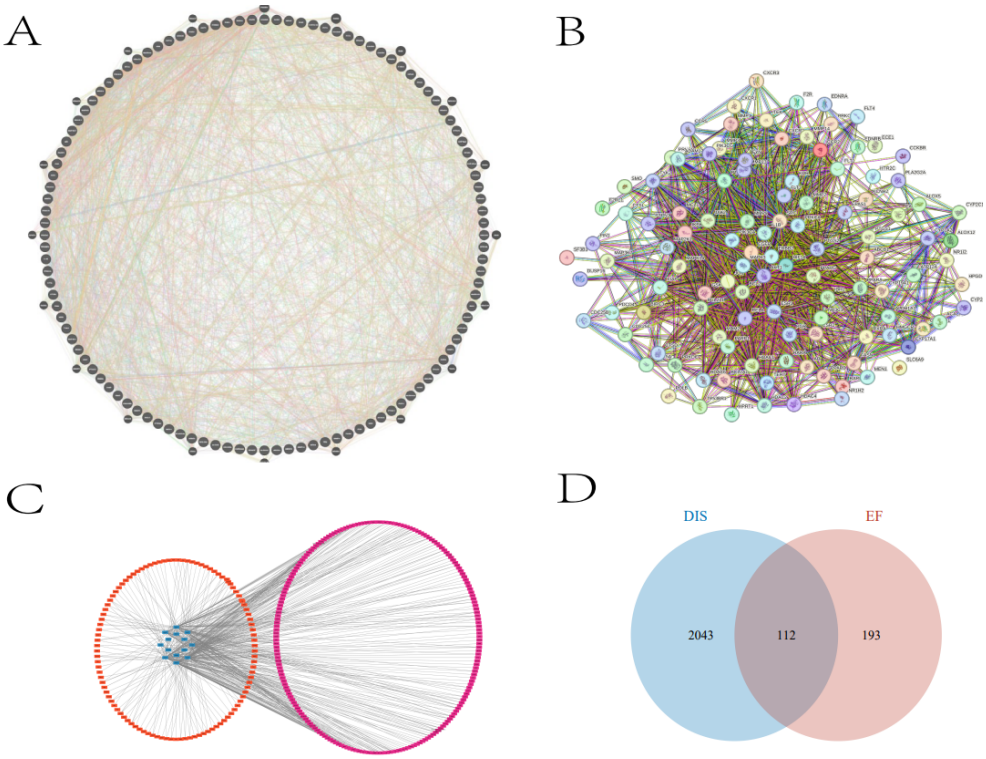

Figure 1. Network analysis of modified Wumei pills and colon cancer targets. This figure displays the network analysis results, including the Genemania network (**A**) showing the intersection of input prescriptions and disease-related genes, the protein-protein interaction (PPI) network map (**B**) of the intersection genes, a network diagram (**C**) for colon cancer highlighting the active ingredients of supplemented Wumei pills and their corresponding intersection targets, and a Venn diagram (**D**) representing the drug targets associated with the diseases under consideration.

A comprehensive search of the GeneCards database yielded a total of 2,155 targets associated with colon cancer. Subsequently, an inquiry into the drag-net database identified an additional 30 genes. The disease targets retrieved from both databases were consolidated and de-weighted, resulting in a cumulative total of 2,156 targets. By intersecting the disease targets with drug targets, it was determined that 112 disease targets related to colon cancer can be effectively targeted by the modified Wumei pill.

The Cytoscape 3.9.0 software was employed to create a network diagram illustrating the relationship between "Supplemented Wumei Pills, effective ingredients, and the intersection targets related to colon cancer. Based on the degree of intersection and the interactions among the targets, six target genes were selected, each exhibiting an interaction value greater than 6. The primary therapeutic targets identified for colon cancer in relation to the Cherry and Plum Pill include ADRA2B, CXCR3, CYP19A1, NR1H2, PAPPA, and PGR.

The dual focus of the supplemented Wumei pill and colon cancer was analyzed using the String database, with Homo sapiens selected as the species of interest. A medium confidence threshold of 0.400 was established, resulting in the identification of 49 nodes. The analysis revealed a total of 328 edges, an average node degree of 13.4, and an average local clustering coefficient of 0.633. The protein-protein interaction (PPI) rich set exhibited a significance level of P < 10^-16. This data was utilized to construct a protein interaction network diagram illustrating the common targets associated with modified Wumei pills and colon cancer.

The input will be utilized to construct the Genemania network intersection diagram, which will allow for the identification of the genes ADRA2B, CXCR3, CYP19A1, NR1H2, PAPPA, and PGR, exhibiting the highest degree of crosslinking among all intersecting genes.

3.2. GO Enrichment and KEGG Enrichment Diagram

As depicted in **Figure 2**, the Gene Ontology (GO) enrichment analysis of the intersection genes identified via the Venn diagram reveals significant enrichment in multiple biological processes. Notably, these processes encompass "intracellular receptor signaling pathway," "response to chemical stress," and "response to oxidative stress." In terms of cellular components (CC), the enrichment analysis indicates that these genes are predominantly associated with "membrane rafts," "membrane microdomains," and "membrane regions." Regarding molecular function (MF), the results demonstrate that these genes are primarily linked to "nuclear receptor activity," "ligand-activated transcription factor activity," and "DNA-binding transcription factor binding." Furthermore, the gene pathway network interaction map elucidates the relationships of these genes with various pathways, including the "TNF signaling pathway," "endocrine resistance," "chemical carcinogen-receptor activation," and "atherosclerosis."

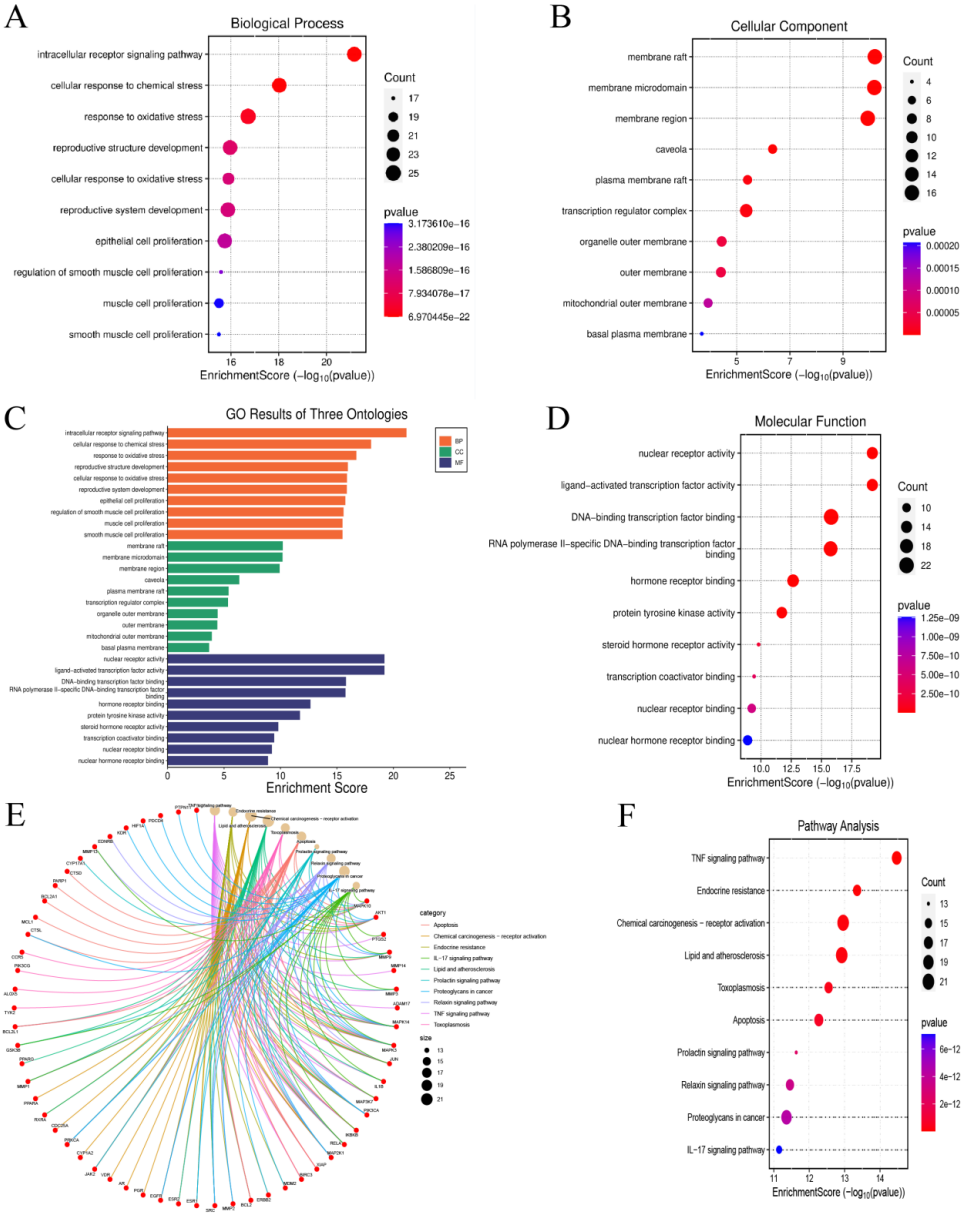

Figure 2. GO enrichment and KEGG enrichment analysis. The figure presents a functional bubble diagram for (**A**) Biological Processes (BP); (**B**) Cellular Components (CC); (**C**) a histogram of Gene Ontology (GO) enrichment

pathways; (**D**) a functional bubble diagram for molecular function (MF); (**E**) a network diagram illustrating gene-pathway construction; (**F**) a bubble diagram for KEGG pathways.

3.3. Immunohistochemical Images

The immunohistochemical results presented in **Figure 3** indicate that the genes ADRA2B, CXCR3, CYP19A1, NR1H2, PAPPA, and PGR are significantly expressed in the colon tissues of patients with colon cancer. Notably, the ADRA2B gene exhibits high expression levels in both tumor cells and immune cells within the tumor microenvironment, including macrophages and chromaffin cells. The expression of the CYP19A1 gene in colon cancer tissues appears to involve both tumor cells and endothelial cells. Furthermore, the expression of the NR1H2 gene is observed in tumor cells associated with colon cancer as well as in immune cells within the tumor microenvironment. The expression of the PAPPA gene in colon cancer tumor cells is linked to tumor growth and metastasis, whereas the expression of the PGR gene is primarily confined to tumor cells. Additionally, the CXCR3 gene is predominantly expressed in activated T cells and natural killer cells.

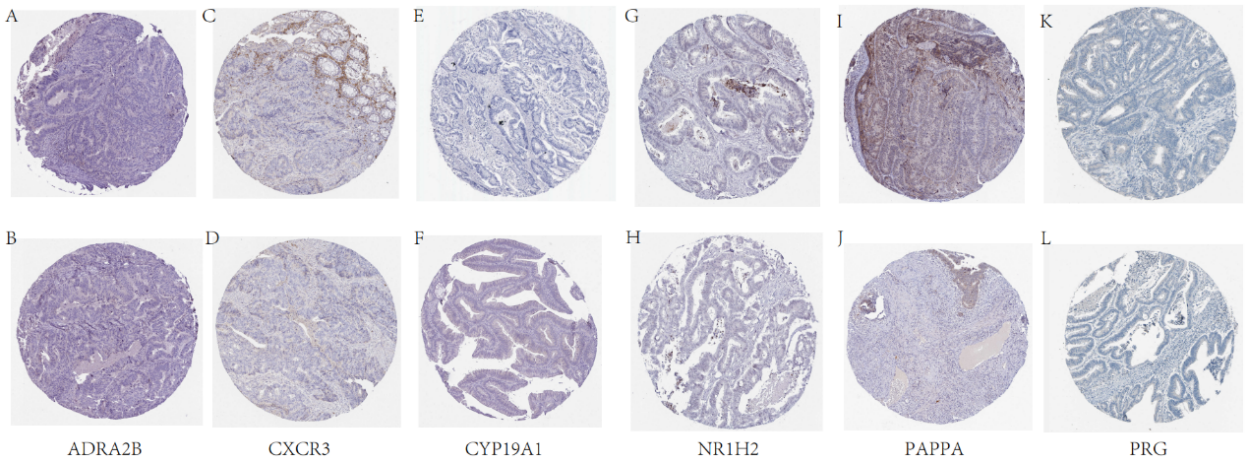

Figure 3. Immunohistochemical images. (**A**,**B**) Immunohistochemical staining of ADRA2B in tissue samples; (**C**,**D**) Immunohistochemical staining of CXCR3 in tissue samples; (**E**,**F**) Immunohistochemical staining of CYP19A1 in tissue samples; (**G**,**H**) Immunohistochemical staining of NR1H2 in tissue samples; (**I**,**J**) Immunohistochemical staining of PAPPA in tissue samples; (**K**,**L**) Immunohistochemical staining of PRG in tissue samples. This figure shows immunohistochemical results indicating the expression of genes ADRA2B, CXCR3, CYP19A1, NR1H2, PAPPA, and PGR in colon tissues of patients with colon cancer.

3.4. ROC Curve

Supported by the information presented in the Receiver Operating Characteristic (ROC) curve depicted in **Figure 4**, we can assess the prognostic significance of these six genes in colon cancer. The ROC curve serves as a valuable tool for evaluating the performance of a binary classification model by comparing the true positive rate (sensitivity) with the false positive rate (1-specificity), thereby illustrating the model's classification ability across various thresholds. The area under the curve (AUC) quantifies the overall performance of the ROC curve, with values ranging from 0 to 1. A value approaching 1 signifies superior classification capability, while a value of 0.5 indicates a lack of classification ability. In the context of the six genes analyzed, the ADRA2B gene exhibits an AUC value of 0.609, suggesting a moderate capacity to differentiate between colon cancer and non-colon cancer samples. The CXCR3 gene presents an AUC value of 0.529, which implies limited prognostic efficacy in distinguishing colon cancer from non-colon cancer samples. Conversely, the CYP19A1 gene demonstrates a relatively high AUC value of

0.777, indicating strong efficacy in prognostic assessment for colon cancer. The NR1H2 gene has an AUC value of 0.698, reflecting its potential prognostic value in differentiating colon cancer patients. The PAPPA gene shows an AUC value of 0.581, suggesting a moderate prognostic capability. Finally, the PGR gene achieves an AUC value of 0.904, indicating that it possesses the strongest prognostic correlation among the six genes evaluated.

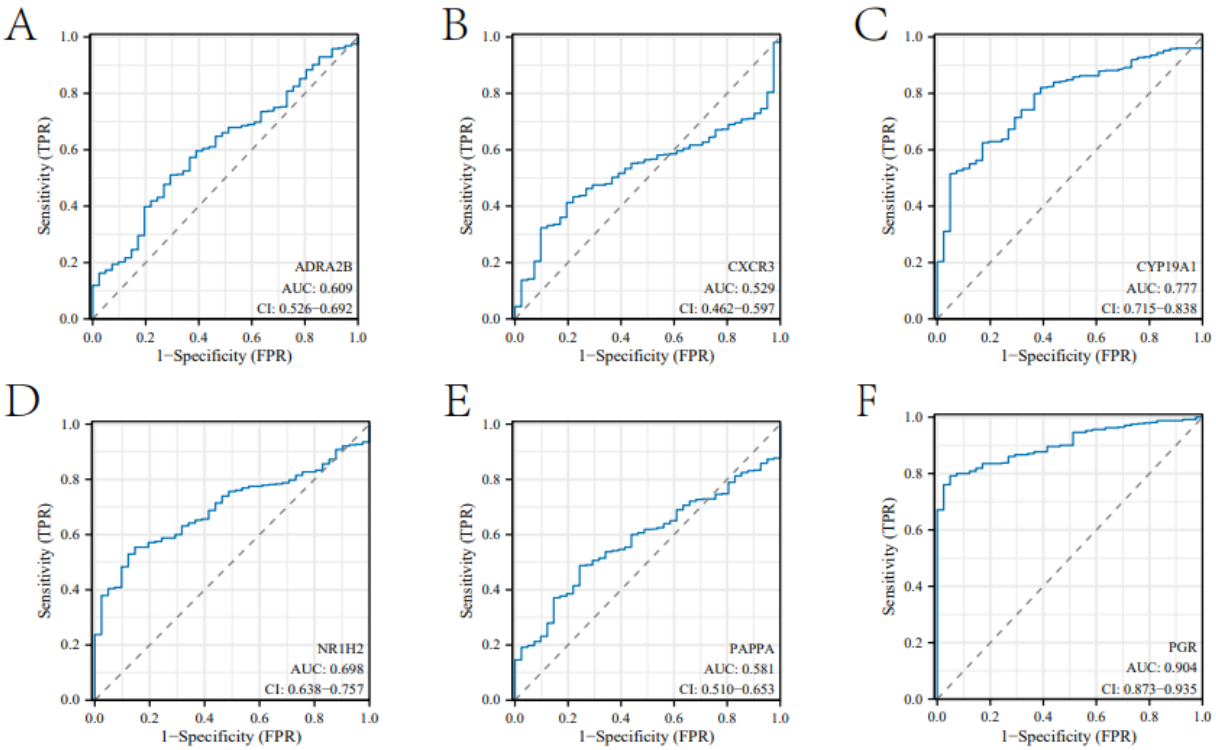

Figure 4. ROC curve analysis. (**A**) Receiver Operating Characteristic (ROC) curve of ADRA2B with an area under the curve (AUC) of 0.609 and confidence interval (CI) of 0.526–0.692; (**B**) ROC curve of CXCR3 with an AUC of 0.529 and CI of 0.462–0.597; (**C**) ROC curve of CYP19A1 with an AUC of 0.777 and CI of 0.715–0.838; (**D**) ROC curve of NR1H2 with an AUC of 0.698 and CI of 0.638–0.757; (**E**) ROC curve of PAPPA with an AUC of 0.581 and CI of 0.510–0.653; (**F**) ROC curve of PGR with an AUC of 0.904 and CI of 0.873–0.935. The Receiver Operating Characteristic (ROC) curve analysis is depicted, evaluating the prognostic significance of the six genes in colon cancer, with the area under the curve (AUC) values indicated for each gene.

3.5. KM Curve Diagram

As illustrated in **Figure 5**, the PFI curve for ADRA2B exhibits a small p-value; however, no significant difference is observed ($p > 0.05$). For CXCR3, the PFI and OS curves show no significant differences ($p > 0.05$), whereas the DSS curve demonstrates a significant difference with a p-value of 0.039, indicating a notable variation in DSS staging. The DSS, OS, and PFI curves for CYP19A1, PAPPA, and PGR all show no significant differences ($p > 0.05$). In contrast, the DSS and PFI curves for NR1H2 reveal significant differences ($p < 0.05$).

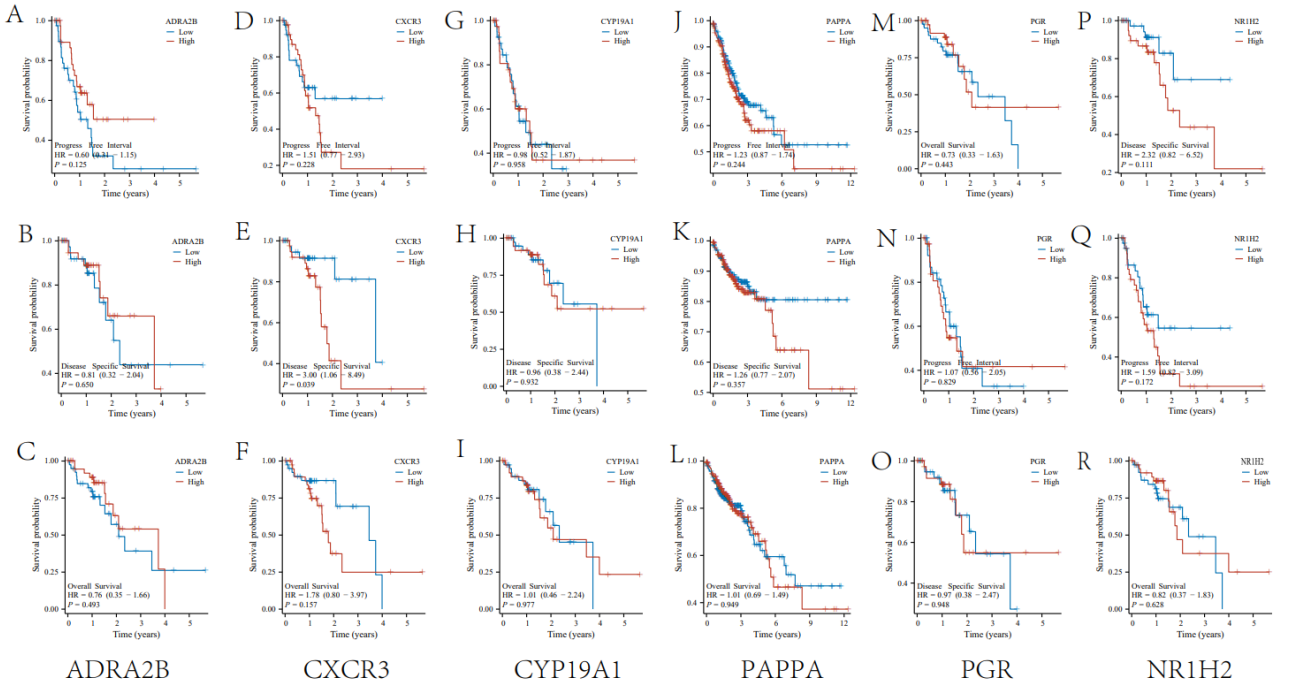

Figure 5. KM curve analysis. (**A**) Progression-free survival (PFS) curve of ADRA2B; (**B**) Disease-specific survival (DSS) curve of ADRA2B; (**C**) Overall survival (OS) curve of ADRA2B; (**D**) PFS curve of CXCR3; (**E**) DSS curve of CXCR3; (**F**) OS curve of CXCR3; (**G**) PFS curve of CYP19A1; (**H**) DSS curve of CYP19A1; (**I**) OS curve of CYP19A1; (**J**) PFS curve of PAPPA; (**K**) DSS curve of PAPPA; (**L**) OS curve of PAPPA; (**M**) PFS curve of PGR; (**N**) DSS curve of PGR; (**O**) OS curve of PGR; (**P**) PFS curve of NR1H2; (**Q**) DSS curve of NR1H2; (R) OS curve of NR1H2. Kaplan-Meier (KM) survival curves are depicted for the genes ADRA2B, CXCR3, CYP19A1, NR1H2, PAPPA, and PGR, highlighting their prognostic significance in terms of Progression-Free Interval (PFI), Disease-Specific Survival (DSS), and Overall Survival (OS).

3.6. Comparison of Differences between Disease and Non-Disease

According to the data presented in **Figure 6**, a comparative analysis of gene expression between colon cancer tissues and normal tissues reveals several noteworthy findings. Firstly, the expression level of the ADRA2B gene was significantly elevated in colon cancer tissues compared to normal tissues ($p < 0.05$). This increase suggests that ADRA2B may play a critical role in the development or progression of colon cancer, with its up-regulation potentially linked to various tumor biological behaviors, including growth, invasion, and metastasis. Conversely, the expression level of the CXCR3 gene did not exhibit a statistically significant difference between normal and colon cancer tissues ($p > 0.05$). This finding implies that CXCR3 may not be a major contributor to the onset of colon cancer, or its involvement may be restricted to specific subtypes or stages of the disease, necessitating further investigation to elucidate its role in colon cancer. Additionally, the expression level of the CYP19A1 gene in colon cancer tissues demonstrated a statistically significant increase ($p < 0.05$), indicating its potential involvement in the pathogenesis of colon cancer, particularly concerning the proliferation and survival of tumor cells. The NR1H2 gene also showed a significant difference in expression between normal and colon cancer tissues ($p < 0.05$), suggesting that NR1H2 may be implicated in critical biological processes associated with colon cancer, including cell signaling, metabolic regulation, and immune response. In contrast, the expression of the PAPPA gene did not reveal a significant difference between normal and colon cancer tissues ($p > 0.05$). Notably, the expression level of the PGR gene was found to be higher in normal tissues than in colon cancer tissues, with this difference being statistically significant ($p < 0.05$). This observation may indicate that the down-regulation of PGR in colon cancer is associated with tumor inhibition or progression, warranting further investigation into its specific mechanisms of action within the context of colon cancer.

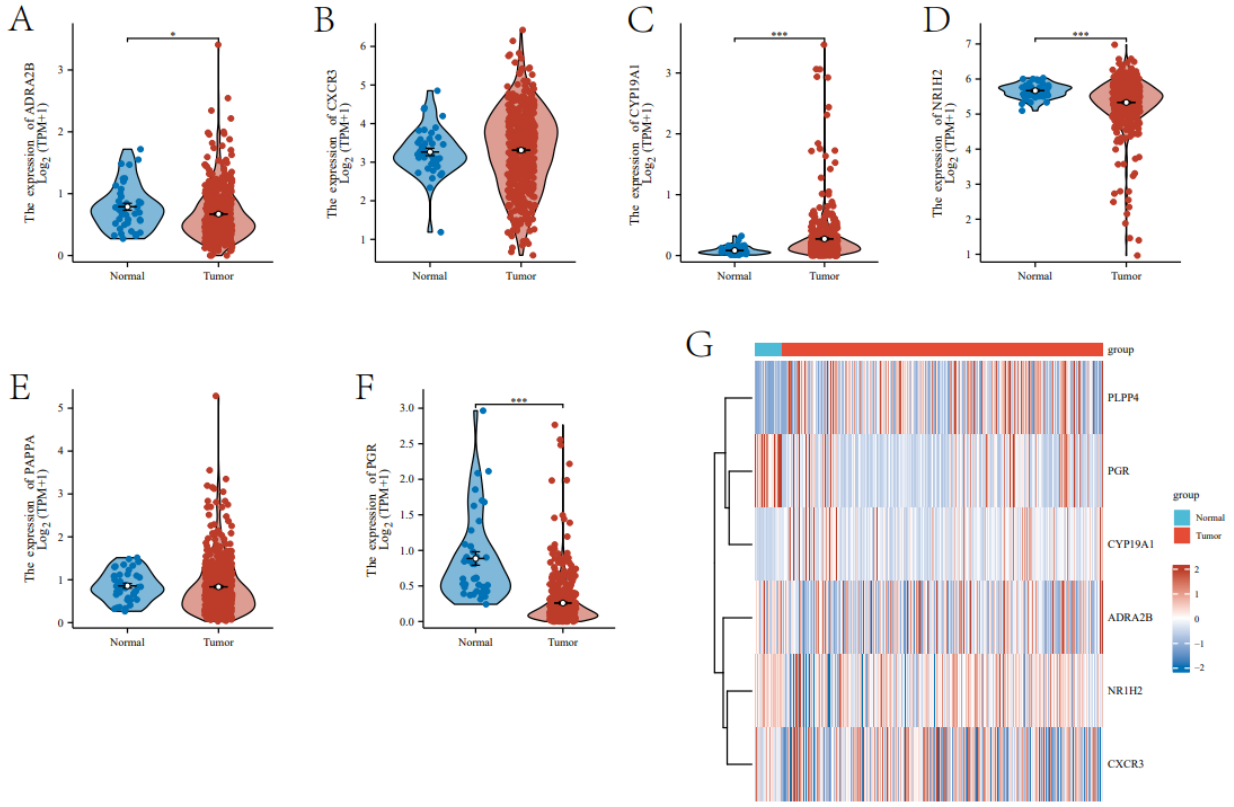

Figure 6. Gene expression comparison between disease and non-disease tissues. (**A**) The expression of ADRA2B in normal and tumor tissues; (**B**) The expression of CXCR3 in normal and tumor tissues; (**C**) The expression of CYP19A1 in normal and tumor tissues; (**D**) The expression of NR1H2 in normal and tumor tissues; (**E**) The expression of PAPPA in normal and tumor tissues; (**F**) The expression of PGR in normal and tumor tissues; (**G**) Heatmap of differentially expressed genes between normal and tumor tissues. Comparative analysis of gene expression levels between colon cancer tissues and normal tissues for ADRA2B, CXCR3, CYP19A1, NR1H2, PAPPA, and PGR genes.

3.7. Immune Cell Lollipop Chart

As illustrated in **Figure 7**, a correlation analysis was performed between the principal variable in the dataset and the immune infiltration matrix data. The findings indicate that when NR1H2 serves as the primary variable, immune cells such as natural killer (NK) cells, NK CD56bright cells, and immature dendritic cells (iDC) exhibit significant differences and a positive correlation with both normal and tumor tissues. Conversely, these immune cells demonstrate a negative correlation with central memory T cells (Tcm), Th2 cells, and T helper cells. In instances where progesterone receptor (PGR) is the dominant variable, macrophages, mast cells, iDC, and other immune cells show significant differences and a positive correlation in both normal and tumor tissues, while Th2 cells, NK CD56bright cells, and Th17 cells are negatively correlated. Furthermore, when CYP19A1 is the primary variable, Tcm, macrophages, T helper cells, and other immune cells display considerable differences and a positive correlation with normal and tumor tissues, while they are negatively correlated with activated dendritic cells (aDC), NK CD56bright cells, and Th17 cells. When adrenoceptor alpha 2B (ADRA2B) is the main variable, NK cells, T follicular helper (TFH) cells, iDC, and other immune cells are markedly different and positively correlated with both normal and tumor tissues, while they exhibit a negative correlation with Th2 cells. In the case of C-X-C chemokine receptor type 3 (CXCR3) as the primary variable, regulatory T cells (Treg), NK CD56dim cells, dendritic cells (DC), and other immune cells show significant differences and a positive correlation with normal and tumor tissues, while they are negatively correlated with Th2 cells and Tcm. Lastly, when pregnancy-associated plasma protein A (PAPPA) is the

dominant variable, macrophages, neutrophils, Th1 cells, and other immune cells are notably different and positively correlated with both normal and tumor tissues, while they exhibit a negative correlation with NK CD56bright cells and Th17 cells.

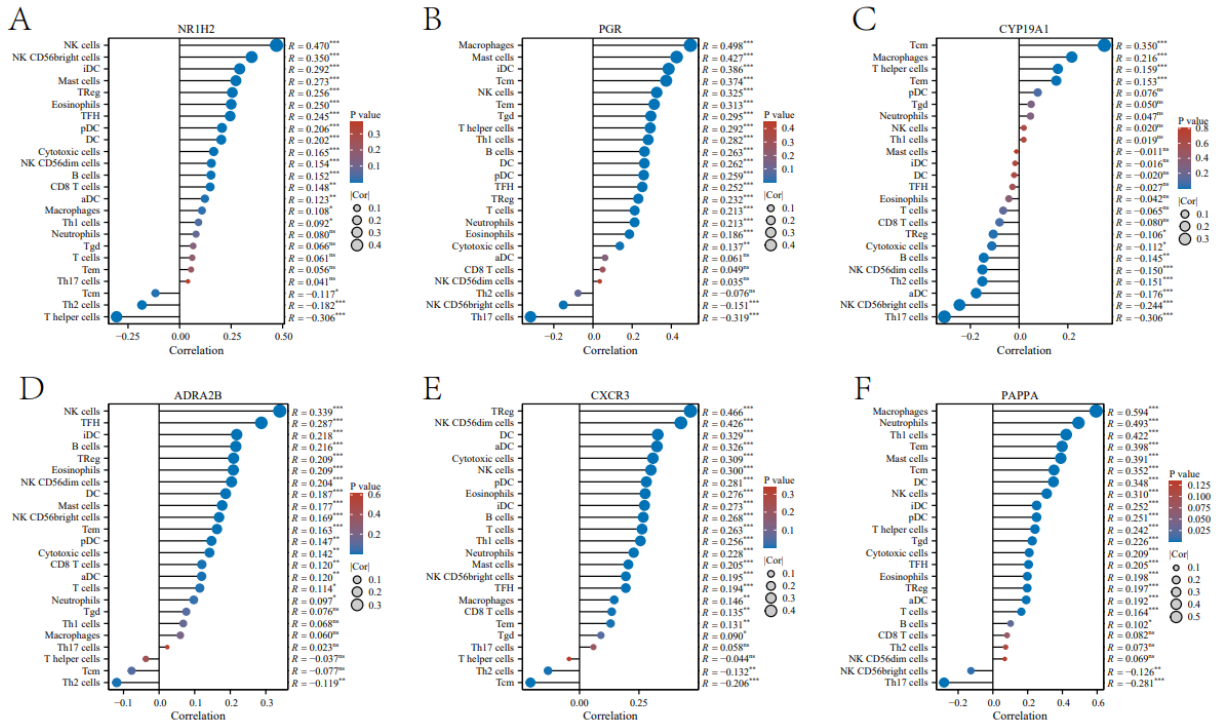

Figure 7. Immune cell lollipop chart. (**A**) Correlation between NR1H2 expression and immune cell infiltration; (**B**) Correlation between PGR expression and immune cell infiltration; (**C**) Correlation between CYP19A1 expression and immune cell infiltration; (**D**) Correlation between ADRA2B expression and immune cell infiltration; (**E**) Correlation between CXCR3 expression and immune cell infiltration; (**F**) Correlation between PAPPA expression and immune cell infiltration. The figure illustrates the correlation between the primary variable in the dataset and the immune infiltration matrix data, showing significant differences and correlations with specific immune cell types.

3.8. Comparison of Immune Cell Groups and Heat Map

As illustrated in **Figure 8**, the immune expression difference map and correlation heat map indicate that when NR1H2 serves as the primary variable, there are significant differences observed in natural killer (NK) cells, NK CD56bright cells, and immature dendritic cells (iDC), among others. Conversely, when progesterone receptor (PGR) is the primary variable, notable differences are evident in macrophages, mast cells, iDC, and other immune cell types between normal and tumor tissues. Additionally, when CYP19A1 is identified as the dominant variable, significant differences are observed in central memory T cells (Tcm), macrophages, T helper cells, and other immune cells in normal versus tumor tissues. Furthermore, when ADRA2B is the principal variable, significant differences are noted in NK cells, T follicular helper (TFH) cells, iDC, and other immune cells between normal and tumor tissues. Lastly, when CXCR3 is the most prominent variable, regulatory T cells (Treg), NK CD56dim cells, dendritic cells (DC), and other immune cells exhibit significant differences between normal and tumor tissues.

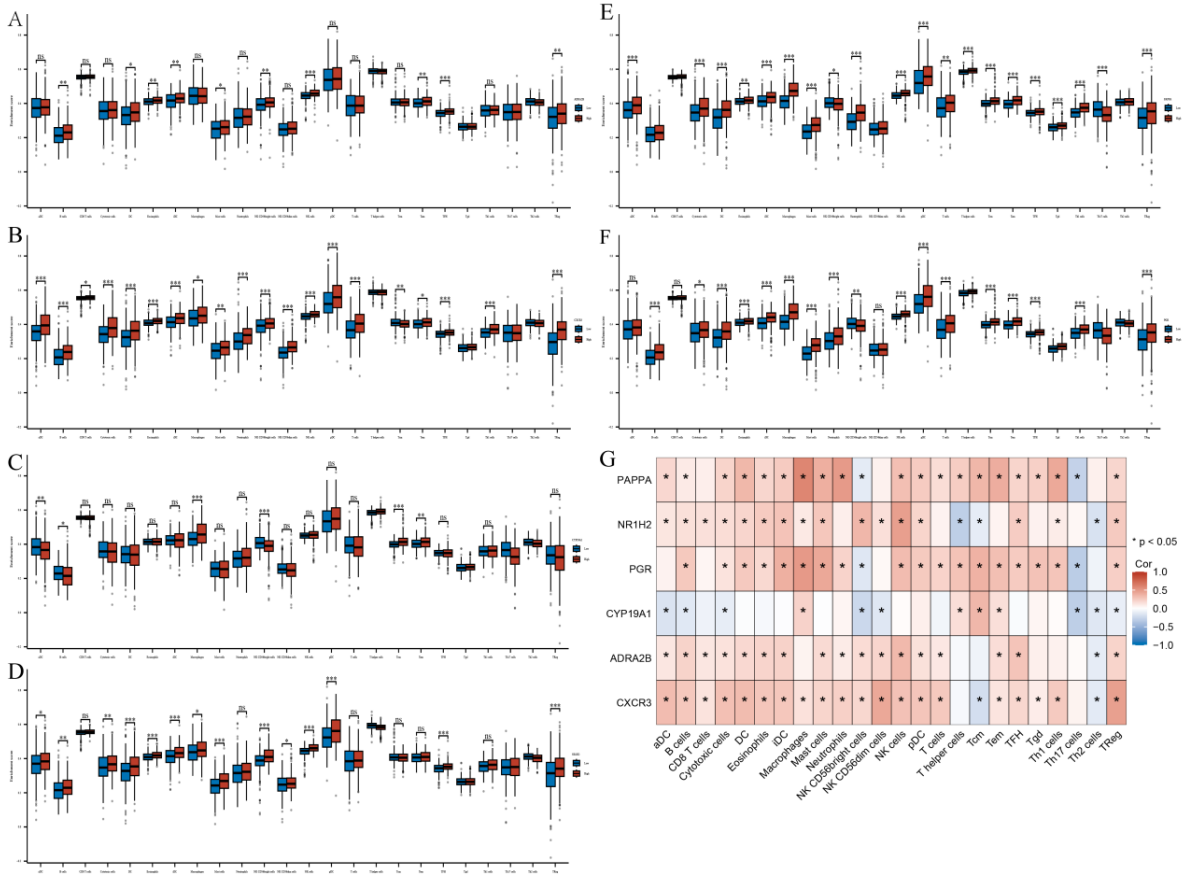

Figure 8. Comparison of immune cell groups and heat map. (**A**) Correlation between ADRA2B expression and immune cell infiltration levels; (**B**) Correlation between CXCR3 expression and immune cell infiltration levels; (**C**) Correlation between CYP19A1 expression and immune cell infiltration levels; (**D**) Correlation between NR1H2 expression and immune cell infiltration levels; (**E**) Correlation between PAPPA expression and immune cell infiltration levels; (**F**) Correlation between PGR expression and immune cell infiltration levels; (**G**) Heatmap showing the correlation between gene expression and immune cell infiltration. This figure presents an immune expression difference map and correlation heat map, indicating significant differences in immune cell populations between normal and tumor tissues for various genes.

3.9. COX Regression

As illustrated in **Table 1**, the results from the COX analysis indicate significant differences in the pathologic node stage among patients with no lymph node metastasis (N0) compared to those with 1-3 lymph node metastases (N1) and those with more than 4 lymph node metastases (N2), with p-values of 0.042 and less than 0.001, respectively. These findings suggest that the prognosis for patients with colorectal cancer deteriorates markedly with the advancement of pathological N stages, highlighting a strong association between the presence of lymph node metastasis and poor prognosis. Regarding the Pathologic M stage, a significant difference was observed between patients without distant metastasis (M0) and those with distant metastasis (M1), with a p-value of less than 0.001. This indicates that the presence of distant metastasis significantly adversely affects the prognosis of colorectal cancer patients. In terms of primary therapy outcomes, the distinction between disease progression and disease stabilization (PD&SD) versus partial and complete response (PR&CR) was highly significant, with a p-value of less than 0.001. This underscores the strong correlation between treatment response and prognosis in colorectal cancer patients, as those achieving a partial or complete response exhibit a markedly better prognosis compared to those whose disease either progresses or remains stable. Furthermore, the analysis of CYP19A1 gene expression levels revealed a statistically significant difference between low and high expression levels, with a p-value of 0.009. This finding suggests that variations in CYP19A1 gene expression may be closely linked to the prognosis of colorec-

tal cancer patients, with high expression potentially correlating with poorer outcomes. This relationship may be attributed to the role of CYP19A1 in tumor growth, metastasis, and hormone synthesis.

Table 1. COX regression analysis.

Characteristics	Total (N)	HR(95% CI) Univariate Analysis	P Value Univariate Analysis	HR(95% CI) Multivariate Analysis	P Value Multivariate Analysis
Pathologic T stage					
T1&T2	94	Reference		Reference	
T3	322	2.576 (1.183–5.612)	0.017	0.598 (0.113–3.162)	0.545
T4	60	7.021 (2.993–16.473)	<0.001	2.971 (0.502–17.582)	0.230
Pathologic N stage					
N0	283	Reference		Reference	
N1	108	1.681 (1.019–2.771)	0.042	0.016 (0.002–0.149)	<0.001
N2	86	4.051 (2.593–6.329)	<0.001	0.071 (0.012–0.434)	0.004
Pathologic M stage					
M0	348	Reference		Reference	
M1	66	4.193 (2.683–6.554)	<0.001	0.750 (0.212–2.652)	0.655
Pathologic stage					
Stage I&Stage II	267	Reference		Reference	
Stage III&Stage IV	199	2.947 (1.942–4.471)	<0.001	111.677 (10.466–1191.655)	<0.001
Primary therapy outcome					
PD&SD	29	Reference		Reference	
PR&CR	221	0.094 (0.049–0.182)	<0.001	0.100 (0.036–0.278)	<0.001
PAPPA	477				
Low	239	Reference		Reference	
High	238	1.158 (0.785–1.708)	0.460		
NR1H2	477				
Low	239	Reference		Reference	
High	238	1.545 (1.042–2.289)	0.030	1.474 (0.637–3.414)	0.365
PGR	477				
Low	239	Reference		Reference	
High	238	1.038 (0.703–1.533)	0.849		
CYP19A1	477				
Low	239	Reference		Reference	
High	238	1.702 (1.141–2.537)	0.009	1.154 (0.430–3.092)	0.776
ADRA2B	477				
Low	239	Reference		Reference	
High	238	1.307 (0.886–1.927)	0.177		
CXCR3	477				
Low	239	Reference		Reference	
High	238	1.026 (0.697–1.511)	0.895		

The table shows the results of the COX regression analysis, indicating significant differences in pathological stages and CYP19A1 gene expression levels in colorectal cancer patients.

3.10. Stacking Diagram of Immune Infiltration

As illustrated in **Figure 9**, the immune stacked bar chart indicates that under conditions of high expression of target genes, there is an increase in the number of specific immune cell types, including M2 macrophages, CD8 T cells, M0 macrophages, resting CD4 memory T cells, resting dendritic cells, and neutrophils, when compared to conditions of low expression of target genes. This observation suggests that these particular populations of immune cells may play a crucial role in the immune response and in the defense against disease. M2 macrophages are significant in anti-inflammatory processes and tissue repair, contributing to the formation of immune memory through the secretion of anti-inflammatory cytokines and the promotion of immune regulation. CD8+ T cells, also referred to as cytotoxic T cells, are essential for recognizing and eliminating virally infected or malignant cells, thereby serving as a vital component of immune surveillance and memory. M0 macrophages represent unactivated or initial-state macrophages that can rapidly activate to perform phagocytosis and antigen presentation upon detecting pathogen-associated molecular patterns (PAMPs) and damage-associated molecular patterns (DAMPs). Resting CD4+ memory T cells are critical for long-term immune memory, as they can respond swiftly to previously encountered antigens, thereby initiating a more rapid and robust immune response. As professional antigen-presenting cells, resting dendritic cells are responsible for capturing, processing, and presenting antigens to T cells, thereby

activating specific immune responses. Neutrophils serve as the frontline defenders of the innate immune system, capable of rapidly migrating to sites of infection or inflammation to eliminate pathogens through phagocytosis and the release of toxic substances.

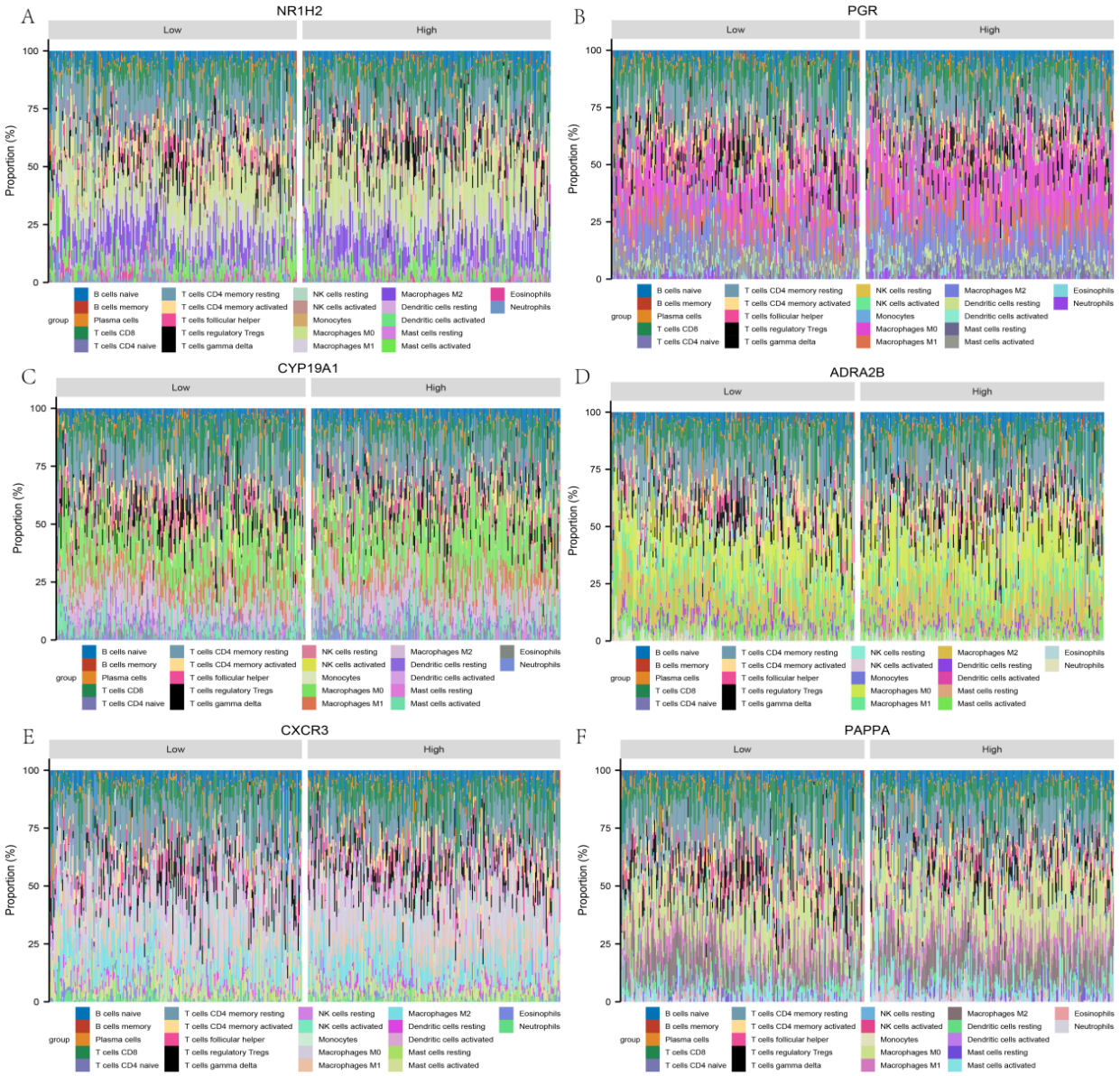

Figure 9. Stacking diagram of immune infiltration. (**A**) Comparison of immune cell composition between low and high NR1H2 expression groups; (**B**) Comparison of immune cell composition between low and high PGR expression groups; (**C**) Comparison of immune cell composition between low and high CYP19A1 expression groups; (**D**) Comparison of immune cell composition between low and high ADRA2B expression groups; (**E**) Comparison of immune cell composition between low and high CXCR3 expression groups; (**F**) Comparison of immune cell composition between low and high PAPPA expression groups. The immune stacked bar chart indicates the increase in specific immune cell types under conditions of high expression of target genes compared to low expression conditions.

3.11. Single Cell Cluster Map

As illustrated in **Figure 10**, the analysis of a single cell indicates that the expression levels of genes such as ADRA2B, CXCR3, CYP19A1, NR1H2, PAPPA, and PGR are significantly elevated in various cell types, including blood and immune cells, endothelial cells, muscle cells, and trophoblast cells. These genes are closely associated with the

functional and pathological processes of colon tissue, thereby exerting a substantial impact on the immune defense mechanisms of the colon. In blood and immune cells, the heightened expression of these genes may be linked to immune surveillance, the regulation of inflammatory responses, and the migration and activation of immune cells. Notably, the ADRA2B and CXCR3 genes may play pivotal roles in the transmission of immune signals and cell-cell interactions, which are essential for the timely initiation and effective regulation of immune responses. Furthermore, as a critical component of the intestinal barrier, the elevated expression of genes such as CYP19A1 and NR1H2 in endothelial cells may contribute to the maintenance of intestinal barrier integrity, the regulation of local hormone levels, and the response to inflammatory signals. This, in turn, supports the maintenance of intestinal homeostasis and provides defense against pathogen invasion. The highly expressed genes in muscle cells, including PAPPA and PGR, may be implicated in the regulation of intestinal motility, thereby influencing intestinal peristalsis and secretion, which are crucial for nutrient absorption and waste excretion. Additionally, trophoblast cells play a vital role in nutrient supply and immune regulation during embryonic development. In the context of colon cancer, these cells may be associated with mechanisms of immune evasion and angiogenesis within the tumor microenvironment, thereby influencing tumor progression and prognosis.

Figure 10. Single cell cluster map. The figure illustrates the expression patterns of (**A**) ADRA2B; (**B**) CXCR3; (**C**) CYP19A1; (**D**) NR1H2; (**E**) PAPPA; and (**F**) PGR genes across various cell types, highlighting their roles in immune defense mechanisms and tumor development.

3.12. Molecular Docking and Molecular Dynamics Simulation

As illustrated in **Figure 11**, the results of the molecular docking studies offer a quantitative evaluation of the binding affinity of the active pharmaceutical ingredient Diop to various target proteins. The data indicate that the

binding energies of Diop with the proteins ADRA2B, CXCR3, CYP19A1, NR1H2, PAPPA, and PGR are −9.5, −34.6, −10.8, −10.2, −9.2, and −10.0 kcal/mol, respectively. In the context of molecular docking, binding energy serves as a critical parameter for assessing the strength and stability of the interaction between the ligand (the active substance) and the receptor (the target protein). The findings of this study reveal that the binding energy of Diop to all aforementioned target proteins is less than zero, suggesting that the interaction between Diop and these proteins is stable and indicative of potential pharmacological activity. Notably, the binding energy of Diop with CXCR3 is −34.6 kcal/mol, representing the strongest interaction among those analyzed, which implies a significant interaction between Diop and CXCR3. This robust interaction may have substantial implications for drug design and optimization, as stronger binding is often correlated with enhanced drug potency and selectivity.

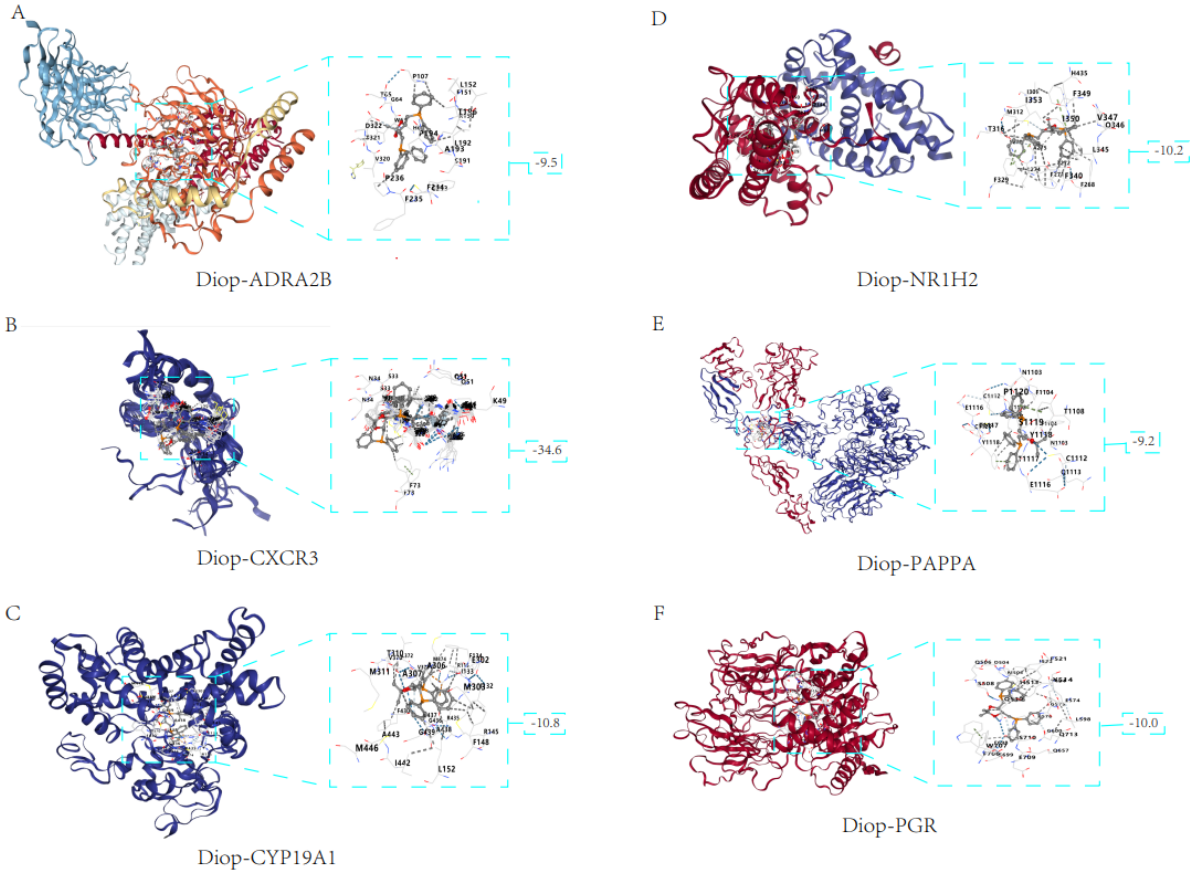

Figure 11. Molecular docking analysis. (**A**) Molecular docking analysis of Diop with ADRA2B; (**B**) Molecular docking analysis of Diop with CXCR3; (**C**) Molecular docking analysis of Diop with CYP19A1; (**D**) Molecular docking analysis of Diop with NR1H2; (**E**) Molecular docking analysis of Diop with PAPPA; (**F**) Molecular docking analysis of Diop with PGR. Molecular docking results are presented, offering a quantitative evaluation of the binding affinity of the active pharmaceutical ingredient Diop to various target proteins, with binding energies indicated.

As shown in **Figure 12**, each RMSD value represents the degree of structural change of DIOP molecule and specific protein (ADRA2B, CXCR3, CYP19A1, NR1H2, PAPPA, PGR) complex in the simulation process is stable, and the complex structure of DIOP molecule and these proteins changes little. May indicate strong binding stability; A higher RMSD value may indicate a larger structural change, possibly related to ligand binding dynamics or the flexible region of the protein.

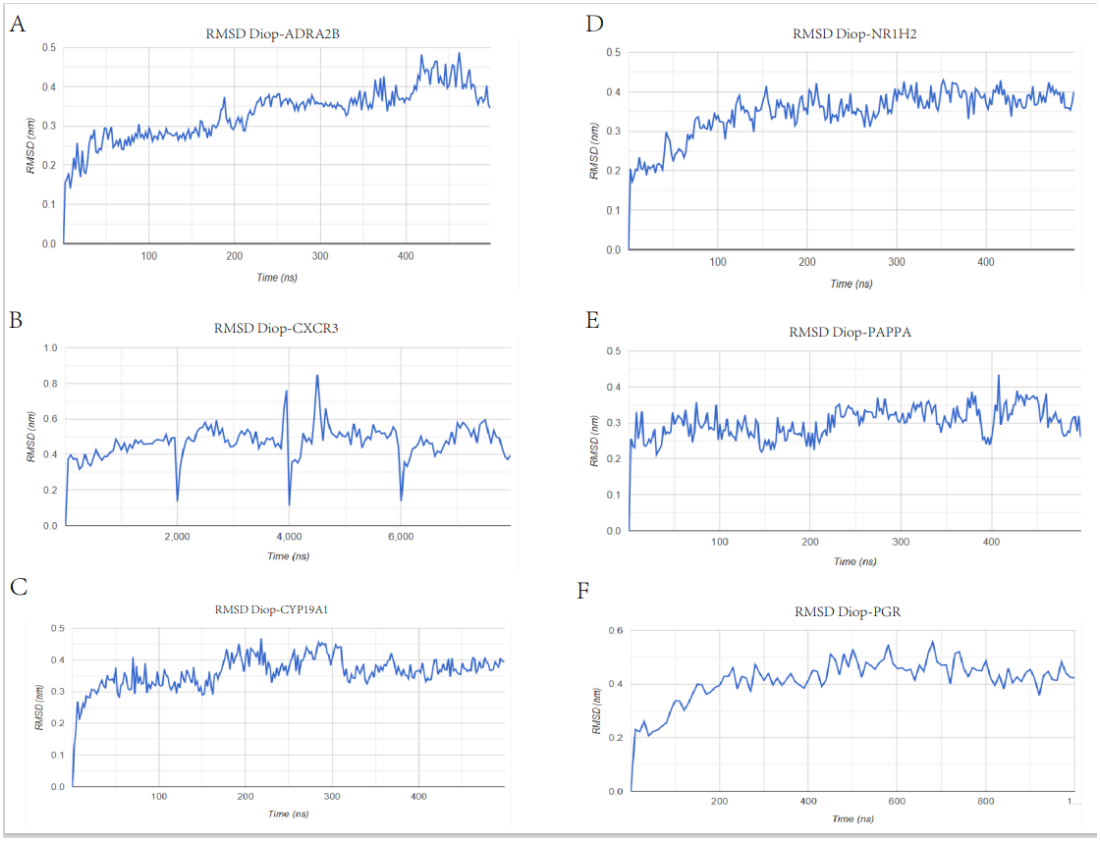

Figure 12. RMSD (root mean square deviation) value.

4. Discussion

The pathological progression of colon cancer is primarily attributed to the damage sustained by colon epithelial cells, coupled with the proliferation and activation of colon stem cells (CSCs), which subsequently differentiate into tumor cells. This process results in an excessive accumulation of extracellular matrix (ECM) components and inflammatory factors within the tumor microenvironment (TME) [12, 13]. Initially normal colon stem cells undergo genetic and epigenetic alterations, as well as modifications in inflammatory factors, growth factors, and ECM components present in the microenvironment, ultimately acquiring malignant phenotypes [14, 15]. These activated colon stem cells exhibit enhanced proliferative capabilities and acquire the ability to undergo epithelial-mesenchymal transition (EMT), facilitating metastasis and tumor formation within colon tissue. As tumors continue to grow, the ECM within the TME becomes excessively deposited, creating a physical barrier that not only supports tumor growth and invasion but also provides essential nutrients and protection for tumor cells, thereby promoting tumor progression and deterioration of tumors. Some studies have shown that Chinese medicine is effective in delaying and treating colon cancer [16, 17]. Chinese medicine prescription supplemented Wumei Pill is a Chinese medicine prescription that adds medicinal materials on the basis of traditional Wumei pill. Plum: As a splendid medicine, has the effect of acid to collect ascaris. Asarum: warm viscera, dispel cold, dispel insects and relieve pain. Dried ginger: warm viscera and dispel cold. Coptis: bitter down ascaris, clearing heat and drying dampness. Yellow cedar: clearing heat and drying dampness. Aconite (preparation): warming viscera and dispelling cold. Cassia twig: warm viscera and dispel cold. Ginseng: invigorating qi and nourishing blood. Angelica: invigorating Qi and nourishing blood. Shu pepper: warm viscera, dispel cold, dispel insects and relieve pain. Honey (refining): Used to make honey pellets. It is operational in the treatment of colon cancer.In this study, the chemical components of 126 supplemented Wumei pills were screened through TCMSP database, and the ADME parameters were set as oral bioavailability (OB) > 30% and pharmacologist (DL) > 0.18.

Among them, 8 chemical components of Wumei, 8 chemical components of asylum, 5 chemical components of

dried ginger and 2 chemical components of angelica sentences were screened. There are 22 chemical components of aconite, 7 chemical components of cassia twig, 39 chemical components of Phellodendron rhododendron, 13 chemical components of Coptis coptis, 21 chemical components of ginseng, and a total of 8 chemical components are screened as active ingredients according to oral bioavailability (OB) > 36% (Diop, Stigmasterol, stigmasterol, etc.). beta-sitosterol, Inermin, Chrysanthemaxanthin, Celabenzine, Deoxyharringtonine, Dianthramine) [1, 18]. The 8 effective active ingredients after screening were imported into the Swiss Target Prediction database to predict the target corresponding to the applicable active ingredients of modified Wumei pills, and 305 genes of the ingredients were screened. By searching the GeneCards database, a total of 2155 colon cancer targets were obtained, and then searching the drag-net database, a total of 30 genes were obtained [3, 19].

The disease targets obtained from the two databases were summarized and de-weighted, and a total of 2156 targets were obtained. The intersection of disease targets and drug targets can obtain 112 disease targets of Supplemented Wumei pill for the treatment of colon cancer by using Cytoscape3.9.0 software to construct the network diagram of "Supplemented Wumei pill - Active ingredients - Intersection targets - colon cancer". According to the degree of overlap and targets related to screen available (interactive value is greater than 6) six target gene analysis results show that the cherry and plum pill for colon cancer six before the main therapeutic targets for the ADRA2B, CXCR3, CYP19A1, NR1H2, PAPPA, PGR. ADRA2B is a G-protein-coupled receptor that is associated with a variety of physiological processes, including the regulation of immune responses and cell proliferation. In the treatment of colon cancer, ADRA2B may serve as a target to modulate the tumor microenvironment and immune response. CXCR3 is a chemokine receptor that is associated with tumor immune surveillance and inflammatory response.

In colon cancer, CXCR3 may be involved in regulating the tumor immune microenvironment and promoting chemotaxis of immune cells. CYP19A1 is an enzyme involved in the biosynthesis of estrogen. Studies have shown that CYP19A1 may inhibit the proliferation and effector function of CD8+ T cells in colon cancer by up-regulating PD-L1, IL-6 and TGF-β, thereby promoting tumor immune escape. NR1H2 is a nuclear receptor involved in regulating lipid metabolism and inflammatory responses. In colon cancer, NR1H2 may serve as a target for regulating lipid metabolism and anti-inflammatory effects. PAPPA is a metalloproteinase, which is associated with tumor invasion and metastasis. In colon cancer, PAPPA may be involved in regulating the aggressiveness and ability of tumor cells to metastasize. PGR is a nuclear receptor that is associated with regulating a variety of biological processes, including cell proliferation and differentiation. In colon cancer, PGR may act as a target that regulates tumor cell proliferation and differentiation. It is in line with the current research and can be used as a drug target [8, 20].

As illustrated in **Figure 2**, the Gene Ontology (GO) enrichment analysis of the intersection genes identified through the Venn diagram indicates significant enrichment in various biological processes. Notably, these processes include "intracellular receptor signaling pathway, "cell response to chemical stress, and "response to oxidative stress. These biological processes are fundamental for cellular perception and response to external stimuli, involving intricate molecular events and regulatory mechanisms within cells. The intracellular receptor signaling pathway is particularly critical, as it encompasses the binding of signaling molecules to intracellular receptors, which subsequently initiates a cascade of downstream events, including alterations in gene expression and modulation of cellular behavior. The cellular response to chemical stress pertains to the mechanisms by which cells detect and manage harmful chemicals, potentially involving detoxification processes and the activation of protective cellular mechanisms. Furthermore, the response to oxidative stress is associated with the cellular defense against damage caused by reactive oxygen species, which is vital for maintaining the redox balance and preventing oxidative injury. In terms of cellular components (CC), the enrichment analysis revealed that these genes are predominantly associated with "membrane raft, "membrane microdomain, and "membrane region. These membrane-associated structures represent critical functional areas of the cell surface that engage in a variety of cellular processes, including signaling, material transport, and intercellular interactions. Membrane rafts are microdomains within the cell membrane that are enriched in specific lipids and proteins, playing a crucial role in cell signaling. In contrast, membrane microdomains and membrane regions contribute to the local architecture and functionality of the cell membrane, with variations in these structures potentially linked to the onset and progression of various diseases. The enrichment results pertaining to molecular function (MF) indicated that these genes are primarily related to "nuclear receptor activity, "ligand-activated transcription factor activity, and "DNA-binding transcription factor binding. These functions are intricately connected to the regulation of gene expression. Nuclear receptors and transcription factors are central components of the intracellular gene expression regulatory network, modulat-

ing the expression of target genes by binding to specific DNA sequences or ligands, thereby influencing the physiological and pathological states of cells. The findings from the gene-pathway interaction network further elucidate the associations of these genes with pathways such as the "TNF signaling pathway, "endocrine resistance, "chemical carcinogen-receptor activation, and "lipid and atherosclerosis. These pathways are implicated in the onset and progression of various diseases, including inflammatory responses, cancer development, metabolic disorders, and cardiovascular diseases [21]. The TNF signaling pathway is integral to inflammation and immune responses, while endocrine resistance pertains to the inhibition of hormone signaling, which has been observed in numerous metabolic diseases. The chemical carcinogen-receptor activation pathway elucidates the role of chemicals in cancer development through receptor activation, whereas the lipid-atherosclerosis pathway is significantly associated with the pathogenesis of cardiovascular disease [5, 22].

The data presented in **Figure 3** indicate that the ADRA2B gene exhibits high expression levels in both tumor cells and immune cells within the tumor microenvironment, including macrophages and pheochromocytomas. This suggests that ADRA2B may play a significant role in the regulation of tumor growth and angiogenesis. Furthermore, the expression of the CYP19A1 gene in colon cancer tissues appears to involve both tumor cells and endothelial cells, with its function being closely associated with estrogen synthesis, which may directly influence the growth and metastatic potential of tumor cells. Additionally, NR1H2 gene expression is observed in both colon cancer tumor cells and immune cells within the tumor microenvironment, where it is critical for the regulation of lipid metabolism and the inflammatory response, potentially affecting tumor development and progression. The PAPPA gene expression in colon cancer cells is correlated with tumor growth and metastasis, while the expression of the PGR gene appears to be predominantly confined to tumor cells. The CXCR3 gene is frequently expressed in activated T cells and natural killer cells, suggesting a connection to immune cell activity within the tumor immune microenvironment. The expression patterns of these genes underscore their complex roles in the development of colon cancer, encompassing aspects of cell signaling, metabolic regulation, immune response, and the formation of the tumor microenvironment [12, 23].

Figure 6 illustrates that the upregulation of ADRA2B gene expression in colon cancer may be associated with various biological behaviors of the tumor, including growth, invasion, and metastasis. ADRA2B, a G-protein-coupled receptor, has the potential to influence cell cycle progression and apoptosis through multiple signaling pathways, thereby facilitating tumor advancement. Additionally, the increased expression of the CYP19A1 gene may be linked to the pathogenesis of colon cancer, particularly in relation to the proliferation and survival of tumor cells. CYP19A1 is known to inhibit the proliferation and effector functions of CD8+ T cells by upregulating PD-L1, IL-6, and TGF-β, which may promote tumor immune evasion. Furthermore, NR1H2 gene expression in colon cancer may play a role in critical biological processes, including but not limited to cell signaling, metabolic regulation, and immune response. As a nuclear receptor, NR1H2's activation may impact lipid metabolism and inflammatory responses, subsequently influencing tumor development and progression. Notably, the expression level of the PGR gene in normal tissues was found to be significantly higher than that in colon cancer tissues ($p < 0.05$), suggesting that PGR expression is downregulated in colon cancer, which may be associated with tumor inhibition or progression. As a nuclear receptor, PGR is implicated in the regulation of various biological processes, including cell proliferation and differentiation, and may represent a potential target for modulating tumor cell proliferation and differentiation in colon cancer [7, 24].

Figure 7 illustrates that the CXCR3 gene is significantly expressed on the surface of certain malignant tumor cells, facilitating tumor metastasis and invasion through receptor-ligand interactions. CXCR3 has the capacity to modulate the functions of immune effector cells and can exert an anti-tumor effect by binding to its specific ligand at the tumor site. Conversely, the chemotaxis of immune cells to the tumor site mediated by CXCR3 may also enhance the proliferation and migration of tumor cells, which is intricately associated with tumor growth and metastasis. The expression of the NR1H2 gene may be detected in both colon cancer tumor cells and immune cells within the tumor microenvironment, playing a pivotal role in the regulation of lipid metabolism and inflammatory responses, which may influence tumor development and progression. As a nuclear receptor, the PGR gene is implicated in the regulation of various biological processes, including cell proliferation and differentiation, and may serve as a potential target for modulating tumor cell proliferation and differentiation in colon cancer [25, 26]. The immune expression difference map and correlation heat map presented in **Figure 8** further corroborate the findings depicted in **Figure 7**. When NR1H2, PGR, CYP19A1, and ADRA2B were analyzed as primary variables, significant differences

in the expression of specific immune cell populations were observed between normal and tumor tissues, underscoring the relevance of these genes in the immune microenvironment of colon cancer. These genes may affect tumor development and immune evasion by modulating the infiltration and functionality of immune cells [27, 28].

The results of the COX regression analysis presented in **Table 1** indicate a significant impact of both the pathological lymph node stage and the pathological distant metastasis stage on the prognosis of patients diagnosed with colorectal cancer. Furthermore, the analysis of CYP19A1 gene expression levels demonstrated a statistically significant difference between low and high expression groups ($p = 0.009$). This finding suggests that variations in CYP19A1 gene expression may be closely associated with the prognosis of colorectal cancer patients. An increased expression of CYP19A1 may correlate with tumor aggressiveness and a poorer prognosis, potentially due to its involvement in the tumor immune microenvironment.

The stacked bar chart depicting immune cell populations in **Figure 9** illustrates that, in instances of high expression of target genes, there is a notable increase in the prevalence of specific immune cell types, such as M2 macrophages and CD8+ T cells, compared to conditions characterized by low expression of target genes. This observation implies that these particular immune cell populations may play a pivotal role in the immune response and in the defense against disease. M2 macrophages are crucial for anti-inflammatory processes and tissue repair, and they contribute to the establishment of immune memory by secreting anti-inflammatory cytokines and facilitating immune regulation. CD8+ T cells, commonly referred to as cytotoxic T cells, possess the capability to recognize and eliminate virally infected or neoplastic cells, thereby serving as a vital component of immune surveillance and memory [6].

The single-cell cluster depicted in **Figure 10** illustrates the expression patterns of the ADRA2B, CXCR3, CYP19A1, NR1H2, PAPPA, and PGR genes across various cell types. Notably, the expression levels of these genes were significantly elevated in blood and immune cells, endothelial cells, muscle cells, and trophoblast cells. This observation suggests that these genes may play a critical role in the immune defense mechanisms of the colon as well as in tumor development. Furthermore, the expression of these genes may be associated with the activation, proliferation, and differentiation of immune cells, thereby influencing the tumor microenvironment and the overall immune response.

The results of the molecular docking studies presented in **Figure 11** offer a quantitative evaluation of the binding affinity of the drug-active compound Diop to various target proteins. The binding energies of Diop with ADRA2B, CXCR3, CYP19A1, NR1H2, PAPPA, PGR, and other proteins are all less than zero, suggesting that the interactions between Diop and these proteins are stable and indicative of potential pharmacological activity. Notably, the binding energy of Diop with CXCR3 is -34.6 kcal/mol, representing the most robust interaction among those analyzed. This significant interaction may have important implications for drug design and optimization, as stronger binding is often correlated with enhanced drug potency and selectivity.

According to **Figure 12**, we can conclude that in this molecular dynamics simulation study, we have paid attention to the stability and dynamic changes of the complexes of DIOP molecules with six different proteins (ADRA2B, CXCR3, CYP19A1, NR1H2, PAPPA, PGR). By analyzing RMSD values, we were able to assess the structural stability and possible functional effects of these complexes during simulation. The RMSD values of DIOP and ADRA2B provide information on the overall structural changes of the complex during the simulation. The lower RMSD value indicated that the complex maintained high structural stability during the simulation, which may be related to the tight binding of the DIOP molecule to the ADRA2B receptor. The RMSD value of CXCR3 complex reveals its structural dynamics during simulation. CXCR3 is a key immunomodulatory receptor, and its interaction with DIOP may have important effects on its functional status. The RMSD value of CYP19A1 complex reflects the structural changes of the complex during simulation. CYP19A1 plays a key role in hormone synthesis, and its structural stability may have a direct effect on enzyme activity. The RMSD value of the NR1H2 complex provides us with insights into the structural stability of the complex. NR1H2 plays an important role in lipid metabolism, and its interaction with DIOP may affect its regulatory function. The RMSD value of PAPPA complex reveals its structural changes during simulation. The expression and function of PAPPA during pregnancy are closely related to fetal development, and the stability of PAPPA structure may have an important influence on the pregnancy process. The RMSD value of the PGR complex gives us information about the structural stability of the complex. PGR plays a central role in the reproductive system and pregnancy maintenance, and its structural stability is essential for its function.

5. Conclusions

This study employed network pharmacology and bioinformatics methodologies to elucidate the potential mechanisms by which modified Wumei pills may contribute to the treatment of colon cancer. Key target genes, including ADRA2B, CXCR3, CYP19A1, NR1H2, PAPPA, and PGR, were identified, highlighting their significant roles in the progression of colon cancer. The findings suggest that modified Wumei pills may influence tumor growth, the immune microenvironment, and prognosis through the regulation of these genes, thereby offering novel insights for targeted therapy and immunotherapy in the management of colon cancer.

Authors Contributions

Conceptualization, S.L. and G.L.; methodology, G.L.; software, S.L.; validation, G.L., SC,L. and C.L.; formal analysis, R.Z.; investigation, R.Z.; resources, G.L.; data curation, S.L.; writing—original draft preparation, S.L.; writing—review and editing, G.L.; visualization, C.L.; supervision, R,Z.; project administration, S.L.; funding acquisition, G.L. All authors have read and agreed to the published version of the manuscript.

Funding

This study did not receive any funding support.

Institutional Review Board Statement

All data were obtained from public databases.

Informed Consent Statement

All the authors agreed to participate in the study. All authors have consented to the publication of this experimental study.

Data Availability Statement

The datasets generated and analyzed during the current study are available upon reasonable request.

Conflicts of Interests

The authors declare that they have no competing interests.

References

1. Huang, J.; Zheng, Y.; Ma, J.; et al. Exploration of the potential mechanisms of Wumei pill for the treatment of Ulcerative Colitis by network pharmacology. *Gastroenterol. Res. Pract.* **2021**, *2021*, 4227668. [CrossRef]
2. Yeh, M. H.; Chiu, H. P.; Wu, M. C.; et al. Integrated Chinese herbal medicine and western medicine on the survival in patients with colorectal cancer: A retrospective study of medical records. *Evid.-Based Complement. Altern. Med.* **2020**, *2020*, 4561040. [CrossRef]
3. Lu, D. X.; Liu, F.; Wu, H.; et al. Wumei pills attenuates 5-fluorouracil-induced intestinal mucositis through Toll-like receptor 4/myeloid differentiation factor 88/nuclear factor-kappaB pathway and microbiota regulation. *World J. Gastroenterol.* **2022**, *28*, 4574. [CrossRef]
4. Wang, J.; Ding, K.; Wang, Y.; et al. Wumei pill ameliorates AOM/DSS-induced colitis-associated colon cancer through inhibition of inflammation and oxidative stress by regulating S-adenosylhomocysteine hydrolase-(AHCY-) mediated Hedgehog signaling in mice. *Oxidative Med. Cell. Longev.* **2022**, *2022*, 4061713. [CrossRef]
5. Sun, Q.; He, M.; Zhang, M.; et al. Traditional Chinese medicine and colorectal cancer: Implications for drug discovery. *Front. Pharmacol.* **2021**, *12*, 685002. [CrossRef]
6. Zhuang, Z.; Wen, J.; Zhang, L.; et al. Can network pharmacology identify the anti-virus and anti- inflammatory activities of Shuanghuanglian oral liquid used in Chinese medicine for respiratory tract infection? *Eur. J. Integr. Med.* **2020**, *37*, 101139. [CrossRef]
7. Zou, Y.; Wang, S.; Zhang, H.; et al. The triangular relationship between traditional Chinese medicines, intestinal flora, and colorectal cancer. *Med. Res. Rev.* **2024**, *44*, 539–567. [CrossRef]
8. Lu, Z. H.; Ding, Y.; Wang, Y. J.; et al. Early administration of Wumei Wan inhibit myeloid-derived suppressor

cells via PI3K/Akt pathway and amino acids metabolism to prevent colitis-associated colorectal cancer. *J. Ethnopharmacol.* **2024**, *333*, 118260. [CrossRef]
9. Zhang, M.; Lu, B. To investigate the molecular mechanism of Wugedan pill in improving insulin resistance based on network pharmacology. *MEDS Chin. Med.* **2022**, *4*, 31–39. [CrossRef]
10. Yin, H.; Liu, W.; Ji, X.; et al. Study on the mechanism of Wumei San in treating piglet diarrhea using network pharmacology and molecular docking. *Front. Vet. Sci.* **2023**, *10*, 1138684. [CrossRef]
11. Shao, S. Y.; Li, Q. Research progress in the treatment of colorectal cancer in classical prescriptions. *TMR Cancer* **2019**, *2*, 200–205. [CrossRef]
12. Fan, Y. H.; Li, T. D.; Gong, R.; et al. Mechanism of Wumei pill in the treatment of non-erosive reflux disease from the perspective of network pharmacology and molecular docking. *Asian Toxicol. Res.* **2021**, *3*, 15. [CrossRef]
13. Fu, Y.; Gao, C.; Sun, X.; et al. Study on the mechanism of action of Wu Mei Pill in inhibiting rheumatoid arthritis through TLR4-NF-kappaB pathway. *J. Orthop. Surg. Res.* **2024**, *19*, 65. [CrossRef]
14. Guan, Z.; Zhao, Q.; Huang, Q.; et al. Modified Renshen Wumei decoction alleviates intestinal barrier destruction in rats with diarrhea. *J. Microbiol. Biotechnol.* **2021**, *31*, 1295. [CrossRef]
15. Lin, X.; Yang, X.; Yang, Y.; et al. Research progress of traditional Chinese medicine as sensitizer in reversing chemoresistance of colorectal cancer. *Front. Oncol.* **2023**, *13*, 1132141. [CrossRef]
16. Lyu, M.; Wang, Y.; Chen, Q.; et al. Molecular mechanism underlying effects of wumeiwan on steroid-dependent asthma: A network pharmacology, molecular docking, and experimental verification study. *Drug Des. Dev. Ther.* **2022**, *16*, 909–929. [CrossRef]
17. Morgan, E.; Arnold, M.; Gini, A.; et al. Global burden of colorectal cancer in 2020 and 2040: incidence and mortality estimates from GLOBOCAN. *Gut* **2023**, *72*, 338–344. [CrossRef]
18. Sun, C.; Xiao, K.; He, Y.; et al. Common mechanisms of Wumei pills in treating ulcerative colitis and type 2 diabetes: Exploring an integrative approach through network pharmacology. *Med. (Baltim.)* **2024**, *103*, e37094. [CrossRef]
19. Wan, Y.; Xu, L.; Liu, Z.; et al. Utilising network pharmacology to explore the underlying mechanism of Wumei Pill in treating pancreatic neoplasms. *BMC Complement. Altern. Med.* **2019**, *19*, 158. [CrossRef]
20. Wei, X.; Leng, X.; Li, G.; et al. Advances in research on the effectiveness and mechanism of Traditional Chinese Medicine formulas for colitis-associated colorectal cancer. *Front. Pharmacol.* **2023**, *14*, 1120672. [CrossRef]
21. Cheng, J.; Zheng, J.; Liu, Y.; et al. Efficacy of traditional Chinese medication Tangminling pill in Chinese patients with type 2 diabetes. *Biosci. Rep.* **2019**, *39*, BSR20181729. [CrossRef]
22. Lee, K.; Choi, Y. J.; Lim, H. I.; et al. Network pharmacology study to explore the multiple molecular mechanism of SH003 in the treatment of non-small cell lung cancer. *BMC Complement. Med. Ther.* **2024**, *24*, 70. [CrossRef]
23. Ma, T.; Ji, P.; Wu, F. L.; et al. Research on the mechanism of Guanyu Zhixie Granule in intervening gastric ulcers in rats based on network pharmacology and multi-omics. *Front. Vet. Sci.* **2024**, *11*, 1390473. [CrossRef]
24. Ni, Z.; Ma, Z.; Qiao, X.; et al. Prediction and analysis of components and functions of Ixeris chinensis based on network pharmacology and molecular docking. *Front. Med.* **2024**, *11*, 1360966. [CrossRef]
25. Wang, T.; Liang, L.; Zhao, C.; et al. Elucidating direct kinase targets of compound Danshen dropping pills employing archived data and prediction models. *Sci. Rep.* **2021**, *11*, 9541. [CrossRef]
26. Yuan, Y.; Hu, H.; Sun, Z.; et al. Combining metagenomics, network pharmacology and RNA-seq strategies to reveal the therapeutic effects and mechanisms of Qingchang Wenzhong decoction on inflammatory bowel disease in mice. *Drug Des. Dev. Ther.* **2024**, *18*, 4273–4289. [CrossRef]
27. Chen, X.; Shi, J.; Lai, Y.; et al. Systematic analysis of randomised controlled trials of Chinese herb medicine for non-alcoholic steatohepatitis (NASH): implications for future drug development and trial design. *Chin. Med.* **2023**, *18*, 58. [CrossRef]
28. Jiang, N.; Li, H.; Sun, Y.; et al. Network pharmacology and pharmacological evaluation reveals the mechanism of the Sanguisorba officinalis in suppressing hepatocellular carcinoma. *Front. Pharmacol.* **2021**, *12*, 618522. [CrossRef]